Chapter 5

Photochemical Production and Release of Gaseous NO_2 from Nitrate-doped Water Ice

C. S. Boxe,[1] A. J. Colussi,[1] M. R. Hoffmann,[1] J. Murphy,[2] P. Wooldridge,[2] T. Bertram,[2] and R. C. Cohen[2]

[1]W. M. Keck Laboratories, California Institute of Technology, Pasadena, CA 91125, and [2]Department of Chemistry and Department of Earth and Planetary Sciences, University of California, Berkeley, California 94720

Abstract

Temperature-programmed NO_2 desorption rates, R, from $NaNO_3$-doped ice irradiated at $\lambda \sim 302$ nm were measured in a continuous flow reactor as function of the nitrate concentration and heating rate, $\partial H = dT/dt$, between $-30 \leq T/^oC \leq 5$. R increases non-monotonically with T reflecting intervening structural transitions of the polycrystalline ice matrix. For $\partial H = 0.70\ ^oC\ min^{-1}$, R noticeably accelerates at ~ –7 ^oC in experiments in which $[NO_3^-]_o > 200\ \mu M$. An additional transition is observed at ~ –23 ^oC at $\partial H = 0.10\ ^oC\ min^{-1}$. Furthermore, samples that were subjected to prolonged photolysis at –30 ^oC continue to evolve NO_2 in the absence of illumination at rates that also surge at ~ –7 ^oC upon heating at $\partial H = 0.70\ ^oC\ min^{-1}$. The total NO_2 released under continuous irradiation does not scale linearly with the duration of the experiment (i.e., with $1/\partial H$), and was observed to vary as $\propto ([NO_3^-]_o)^{½}$, demonstrating the occurrence of significant *in situ* losses of the NO_2 produced in the initial photolytic event prior to desorption. The implications of these results for the interpretation of ambient NO_2 concentrations above ice and snow in polar regions are analyzed.

Submitted (2005): *Journal of Physical Chemistry B*

Introduction

The nearly constant nitrate (e.g., HNO_3, NH_4NO_3, $NaNO_3$) concentrations across snow-covered regions (such the Antarctic ice shelf) suggest remote atmospheric sources,[1,2] that are smoothed out during long-distance transport.[3,4] Thus, if depositional nitrate were ultimately incorporated and preserved in ice cores, [NO_3^-] vs. depth profiles should provide direct and detailed data on global paleoatmospheres.[5,6] It has become apparent, however, that nitrate undergoes solar photolysis in the snowpack leading to NO_x (= NO + NO_2)[7-16] back emissions into the atmospheric boundary layer. Post-depositional transformations, such as reemission or chemical and photochemical degradation, will alter trace gas (i.e., HNO_3, CO_2, H_2O_2, CH_4) imprints thereby compromising their documental value.[6,17] NO_3^- photolysis[18-23] (eqs. 1-3) is also a source of $^{\cdot}OH$ and,[16,24-26] therefore, the oxidation of organic matter within snowpacks is an additional consequence of nitrate photochemistry.[24,26,27]

$$NO_3^- + H^+ \xrightarrow{h\nu} NO_2 + {}^{\cdot}OH \quad (1)$$

$$NO_3^- \xrightarrow{h\nu} NO_2^- + O(^3P) \quad (2)$$

$$NO_2^- + H^+ \xrightarrow{h\nu} NO + {}^{\cdot}OH \quad (3)$$

Previously,[28-30] we showed that frozen NO_3^- is readily photolyzed into NO_2^- and NO_2 within fluid domains (i.e., the quasi-liquid layer, QLL). Quantum yields for NO_2^- and NO_2 formation in ice ($\phi_{NO_2^-} \sim 4.8 \times 10^{-3}$, $\phi_{NO_2} \sim 1.3 \times 10^{-3}$) were similar to those in water ($\phi_{NO_2^-} \sim 6.2 \times 10^{-3}$ and $\phi_{OH} \sim 1.8 \times 10^{-2}$),[22,30] and exhibited Arrhenius behavior between $-35 \leq T/^oC \leq 21$. We also reported that NO_2^- production in frozen media was significantly enhanced in the presence of formate as a co-solute providing further

evidence for non-geminate scavenging of ·OH radicals by formate in extended fluid microdomains.[29] Boxe *et. al.*[28] showed further that NO_x release rates from illuminated frozen nitrate solutions are only partially controlled by molecular photochemistry. Significant amounts of NO_2 remain occluded in subsurficial layers of the frozen medium during photolysis, possibly within interstitial pores at the intersection of ice grains, and only emerge as the ice matrix undergoes discrete metamorphisms.[28]

In this paper, we report temperature-programmed, NO_2 desorption rates measured during the $\lambda \geq 300$ nm photolysis of nitrate-doped polycrystalline ice layers as function of nitrate concentration and heating rates. These new experiments were obtained using LIF detection of NO_2 with pptv sensitivity over a wide range of nitrate concentrations overlapping those representative of typical ice and snow, which complement and corroborate the conclusions drawn from our preliminary study on these systems.[28]

Experimental Methods

A schematic representation of the LIF detection setup, which is directly coupled to the photoreactor[31], is shown in Figure 5.1. Pre-cooled $NaNO_3$ (EM Science) solutions (2 μM, 30 μM, 200 μM, 1 mM, 10 mM, and 50 mM) at pH $\leq$ 6 were sprayed onto a cold finger (CF in Figure 5.2, with exposed area A = 304 cm^2), to produce uniform layers of nitrate-doped polycrystalline ice (NDI). The ice temperature was controlled with an external cryogenic unit (Thermo Neslab ULT-80), which circulated refrigerated fluid through the interior of the CF. The ice-covered CF was encased within a sealed quartz sheath (QS) and placed in a reflective cylindrical stainless steel chamber, and subsequently illuminated by four Hg Pen-Ray UV lamps (UVP, modal 90-0001-04) emitting at $\lambda = 313 \pm 20$ nm. The photon irradiance incident on the QS: $I_i = 3.0 \times 10^{15}$

photons cm^2 s^{-1}, was determined using potassium ferrioxalate as a chemical actinometer.[32] The lamp stability was monitored by a photocell (UDT Sensors, model PIN UV 100L) located on the top of the reflective chamber. The NDI matrices, initially held at ~ –30 ^oC, were heated at three linear ramps (∂H = 0.70, 0.30, and 0.10 ^oC min^{-1}) to 5 ^oC during or, in some specific experiments described below, after irradiation. The NO_2 generated photochemically in the volume enclosed between CF and the QS was continuously flushed with 1 atm zero-air carrier gas, F_c = 2.5 L min^{-1}, into the detection zone.[31] NO_2 fluorescence signals were observed by an LIF detection system with a detection limit of 5 pptv/min.[31]

Results and Discussion

Solutes, such as nitrate, are largely rejected from the ice phase during the freezing of aqueous solutions.[33-40] We have already elaborated on the physical possibilities for the existence of fluid phases and interfaces in frozen solutions.[28] A quasi-liquid layer (QLL) is present at the pristine ice/air interface, and also over contaminated ice samples.[41] However, sub-eutectic phases of low-dimensionality are also present within the bulk of frozen solutions, and they may hold most of the solute impregnating polycrystalline ice.[42-45] Solutes also accumulate in the internal water-vein system at triple junctions (three-grain intersections) and nodes (four-grain intersections),[46-48] as shown by Fukazawa *et al.*[46] using micro-Raman spectroscopy of Antarctic ice samples. They[46] concluded that polar ice is a dynamic environment with fluid-like domains both at the ice-air interface and deep within subsurface regions.

The NO_2 concentrations measured during the photolysis of NDI in the range of 2 μM $\leq [NO_3^-]_o \leq$ 50 mM as function of temperature/time under a ∂H = 0.70 ^oC min^{-1} ramp are

shown in Figs. 5.3a-f. Considering that the LIF detection zone is at ~ 293 K, a constant carrier flow rate of F_c = 2.5 L min^{-1} and an illuminated NDI area of A = 304 cm^2 imply that the detection of 1 pptv (1 part in 10^{12} per volume = 2.5×10^7 molecule cm^{-3} at 1 atm, 293 K) NO_2 in this experimental setup is equivalent to the production of R ~ 3.4×10^6 NO_2 molecules cm^{-2} s^{-1}. It is apparent that the distinct upward inflection observed in [NO_2] at ~ –8 ^oC for [NO_3^-]$_o$ = 50 mM (Fig. 5.3a) gradually disappears at lower nitrate concentrations. Emission rates sharply decrease above ~ –4 ^oC following the depletion of the NO_2 that had accumulated in the interior of the NDI's. The latter effect is a consequence of the fact that upon NDI melting the fluid falls to the bottom of the QS where is only exposed to a small fraction of the actinic radiation. Hence, photolysis rates drop considerably due to geometric factors rather than for photochemical reasons.

Previously, we[28] showed that observations similar to those described above could be rationalized by assuming that most of the photochemically produced NO_2 initially fills microscopic interstices within polycrystalline ice rather than being immediately released into the overlying gas. The NO_2 formed in the network of interconnected cavities that are open to the atmosphere diffuses away concomitantly with photolysis, while the rest remains trapped in closed pockets before effusing through the molecular channels unblocked during the softening of the topmost ice layers at higher temperatures. This hypothesis is fully supported by the experiments shown in Figs. 5.4a,b, in which we illuminated [NO_3^-]$_o$ = 50 mM NDI for 3 hrs at –30 ^oC and then heated the sample at ∂H = 0.70 ^oC min^{-1}. In these experiments, NO_2 concentrations gradually build up, reaching steady-state about > 3 h irradiation. Emissions drop when the photolysis lamps are shut off, and then increase, displaying the distinctive surge at ~ –7 ^oC (cf. Fig. 5.3a). A similar

experiment at $[NO_3^-]_o$ = 2 μM is shown in Figs. 5.5a,b. In this case, average NO_2 emissions at ~ 240 pptv during 3.2 hours represent the production of ~ 3×10^{15} NO_2 molecules, which is equivalent to ~ 50% of the nitrate contained in the ~ 5 cm^3 of the frozen 2 μM $NaNO_3$ solution being photolyzed. The slow decline of NO_2 emissions during the course of the experiment shown in Fig. 5.5a may reflect the gradual depletion of nitrate. The decoupling of photolysis and thermal desorption in these experiments demonstrates the occurrence of two distinct mechanisms for NO_2 release. We notice, however, that NO_2 production rates from $[NO_3^-]_o$ = 50 mM NDI drop ~ 46 times (Figs 5.4a,b), but only a factor of ~ 5 from $[NO_3^-]_o$ = 2 μM NDI (Figs. 5.5a,b) after illumination is halted. In other words, the large ratio of (the largely) photon-driven rates: $R_{50\ mM}/R_{2\ \mu M}$ ~ 29, is not reflected to the ratio of the subsequent purely desorptive dark rates: $R_{50\ mM}/R_{2\ \mu M}$ ~ 4.

An additional indication that nitrate photolysis and NO_2 desorption are not the only processes determining NO_2 release is provided by the $[NO_3^-]_o$-dependence of the total amount of NO_2, $\int [NO_2] F_c dt$, liberated during photolysis over the course of an experiment is proportional to $([NO_3^-]_o)^{1/2}$, at ∂H = 0.70 ^oC min^{-1} (Fig. 5.6). The observed $\int [NO_2] F_c dt \propto ([NO_3^-]_o)^{1/2}$ dependence is not due to the sample becoming optically thick at the highest concentration, since even at $[NO_3^-]_o$ = 50 mM only ~ 1% of the incident photons are absorbed (ε = 7.5 M^{-1} cm^{-1} at 305 nm) by < 300 μm thick frozen layers. Therefore, the fraction of photon flux incident on all our samples that is absorbed by nitrate is linearly proportional to $[NO_3^-]_o$, anticipating a similar dependence for R, at variance with the results of Fig. 5.6, which show a mere ~ 50-fold enhancement of R upon a 2.5×10^4 variation of $[NO_3^-]_o$. A similar argument, based on the small optical

densities that NO_2 reaches in these experiments, indicates that secondary photolysis of NO_2, another complicating feature considered below in more detail, is expected to reduce R by a factor that should be nearly independent of $[NO_3^-]_o$.

A likely explanation of the results of Fig. 5.6 implicates NO_2 reabsorption via the relatively (vs. NO_2 desorption) fast hydrolysis in the quasi-fluid media in which these events take place, reactions 4 or 4':

$$2\ NO_{2\,(aq)} + H_2O_{(l)} \rightarrow NO_3^-{}_{(aq)} + NO_2^-{}_{(aq)} + 2\ H^+{}_{(aq)} \quad (4)$$

$$2\ NO_{2\,(g)} + H_2O_{(l)} \rightarrow NO_3^-{}_{(aq)} + NO_2^-{}_{(aq)} + 2\ H^+{}_{(aq)} \quad (4')$$

Reactions 4 and 4' have the required stoichiometry to produce the $\int [NO_2] F_c dt \propto ([NO_3^-]_o)^{1/2}$ dependence. Equilibrium constants $K_{4'} = 2.8 \times 10^6$, and $K_{4'} = 6.8 \times 10^3$, at 240 K and 270 K, respectively were calculated using $\Delta H_{4'} = -25.7$ kcal mol^{-1} and $\Delta S_{4'} = -77.9$ cal K^{-1} mol^{-1} (in M, atm units)].[49] Assuming pH 5.0, $[NO_3^-] = 50$ mM, $[NO_2^-] \sim 0.1 \times [NO_3^-] = 5$ mM, $[H_2O] = 55$ M, we calculate equilibrium NO_2 pressures of 1.3×10^{-11} atm, and 2.6×10^{-10} atm at 240 K and 270 K, respectively, that are much smaller than the ~ 1 ppbv and 10 ppbv levels shown in Fig. 5.3a at the corresponding temperatures. At $[NO_3^-] = 2\ \mu$M, $[NO_2^-] \sim 1\ \mu$M,[50,51] the equilibrium NO_2 pressures drop ~ 1×10^4 times relative to the above values. Even the occurrence of hundred-fold larger nitrate concentrations in the interstitial fluids, due to solute rejection upon freezing, will not affect the conclusion that NO_2 hydrolysis may be an important and competitive chemical pathway in these systems. The rates of reaction (4) at the low NO_2 concentrations prevalent in present experiments (in which there is minimal dimerization of NO_2 into N_2O_4) are expected to be second order in $[NO_2]$.[52] Thus, the much larger NO_2 levels that

should be produced, in principle, by photolysis of the more concentrated NDI's will be extensively buffered by fast NO_2 hydrolysis via reaction (4). This phenomenon incidentally provides further evidence that chemistry and photochemistry in 'frozen' solutions actually take place in fluid environments, because a 'dry' medium such ice itself would not support NO_2 hydrolysis.

Since the time required to sweep the entire temperature range (from – 30 ^oC to above melting) is inversely proportional to the heating ramp, ∂H, the total amounts of NO_2 collected in photolysis experiments carried out on NDI's of the same composition should be, barring secondary losses, directly proportional to $1/\partial H$, i.e.: $F_c \int [NO_2] dt \propto \partial H^{-1}$. Figs. 5.7a,b show thermograms performed on $[NO_3^-]_o$ = 50 mM NDI at ∂H = 0.30 and 0.10 ^oC min^{-1}, respectively (cf. Fig. 5.3a). These results, in conjunction with those of Fig. 5.3a for ∂H = 0.70 ^oC min^{-1}, as well as those performed on $[NO_3^-]_o$ = 2 μM NDI (not shown), are presented in Fig. 5.8. It is apparent that $F_c \int [NO_2] dt$ vs. ∂H^{-1} plots are not linear: $F_c \int [NO_2] dt$ only increases about threefold upon a sevenfold extension of photolysis time. The inference is that increasingly larger NO_2 losses attain at longer irradiation times. In other words, NO_2 production is not uniquely determined by T and $[NO_3^-]$, but critically depends on the thermal history of the irradiated sample due to the slow kinetics of the processes involved. This phenomena reflect the competition between NO_2 secondary losses and the weak, but positive temperature dependence of its desorption rates. NO_2 is expected to be retained for longer periods within the polycrystalline ice matrix during slower heating schedules and, hence, be subjected to more extensive photodecomposition. We have estimated that the absorption coefficient of NO_2, averaged over the output of our lamps, is ~ 28 times larger than NO_3^-.[30] If NO_2 remained trapped as

a gas, rather than dissolved, the large quantum yield of its photodecomposition in the gas-phase:

$$NO_2 \xrightarrow{h\nu} NO + O(^3P) \qquad (5)$$

$\phi_5 \sim 1$ vs. $\phi_1 \sim \phi_2 \sim 2 \times 10^{-3}$, would further shorten its photodecomposition lifetime. Chemical losses due to secondary radical reactions may also contribute to the non-linearity of Fig. 5.8 plots.[29,30]

Implications for Snowpack Chemistry in Polar Regions

The NO_3^- concentrations measured in snow at rural and remote sites range from 1 to 20 μM.[5,53-56] These overlap with the lower $[NO_3^-]_o$ range of the present experiments. Considering that nitrate samples were subjected to photon irradiances and temperatures of environmental relevance, our results can thus be directly applied to the interpretation of NO_2 emissions from sunlit snow. Chu and Anastasio have recently compared the results of laboratory studies on the photochemistry of frozen nitrate solutions with field measurements of NO_x gases released during spring at various high-latitude locations.[17] Their analysis was based, however, on equating the OH production rates in reaction (1), determined by using benzoic acid as an *in situ* radical scavenger, with the NO_2 rates that should be released into the atmosphere from irradiated snowpacks mimicking their samples. The present experiments show that NO_2 desorption is not instantaneous and that, while trapped in the ice, NO_2, a primary photochemical product of reaction (1), undergoes extensive losses via several chemical and photochemical reaction channels. The inference is that Chu and Anastasio almost certainly overestimated NO_2 fluxes from illuminated snowpacks, and the apparent agreement they obtained between field and laboratory data is probably fortuitous. We suggest that it would be still possible to

reconcile most findings if primary NO_2 were transformed into NO, and/or NO_2^-/HONO species that could be eventually released into the boundary layer, and therefore accounted for as NO_x, depending on the acidity of the local molecular environment.

Conclusions

The photolysis of nitrate embedded within polycrystalline ice produces NO_2(g) that is detected as it emerges from the solid. NO_2 desorption rates under continuous illumination increase with rising temperature, and display distinct acceleration stages that are ascribed to structural transitions of the ice matrix. The amount of NO_2 photodesorbed in a given experiments after scanning the entire temperature range: $-30 \leq T/^oC \leq 5$, scales nonlinearly with $[NO_3^-]_o$ or the heating rate, ∂H. These behaviors express the occurrence of extensive chemical and photochemical losses of NO_2 prior to desorption into the gas-phase.

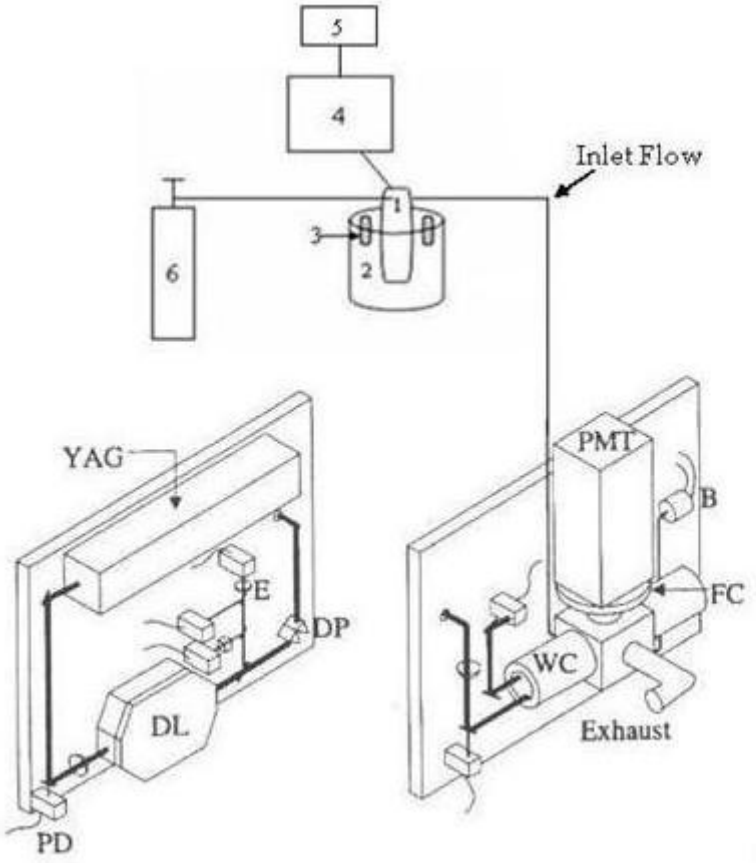

Figure 5.1. Schematic diagram of the experimental setup. (1) photolysis cell (see Figure 5.2); (2) reflective reaction chamber; (3) pen-ray UV lamps emitting at $\lambda_{max} \approx 313$ nm; (4) circulating cryostat; (5) computer workstation utilizing Thermo Neslab Nescom Software; (6) zero air carrier gas. Schematic of the UC, Berkeley laser-induced fluorescence NO_2 instrument was extracted with modifications from Thornton et al. (2000).[31] The core of the instrument is mounted on a breadboard, one side holding the laser subsystem and the other side the detection axis. A frequency doubled Nd^{3+}:YAG laser (YAG) at 532 nm pumps a custom-built dye laser (DL), the output (585 nm) of which is sampled by fused silica beam splitters to monitor power, frequency (by measuring transmittance through an NO_2 reference cell shown as a cube), and line width measured with an external etalon (E). Six photodiode detectors (PD) are used to measure laser power at various points along the beam path. A set of dispersion prisms (DP) is used to separate the 585 nm light from the 532 nm light which is then dumped. The 585 nm light is then sent through a hole in the breadboard to the detection side to the multipass White Cell (WC). The pressure in the WC is measured with a manometer., 100 Torr Baratron (B). NO_2 fluorescence is collected and sent through a series of optical filters

housed in the filter changer (FC) to the photomultiplier tube in its TE-cooled housing (PMT).

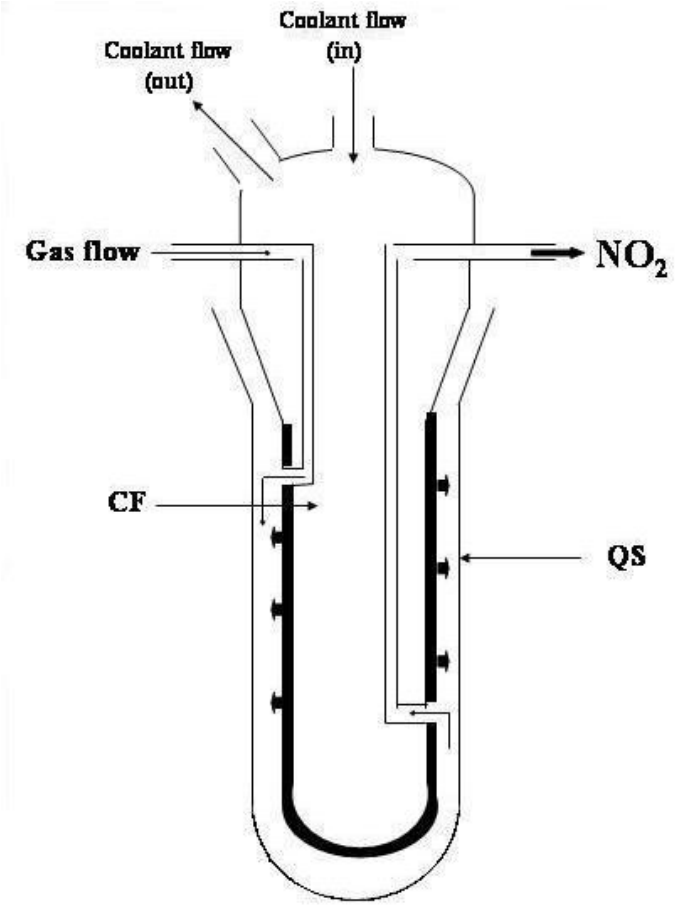

Figure 5.2. The photochemical reaction cell is illustrated above where CF is the inner coldfinger on which polycrystalline ice is formed, and QS is a quartz sheath that encase the coldfinger.

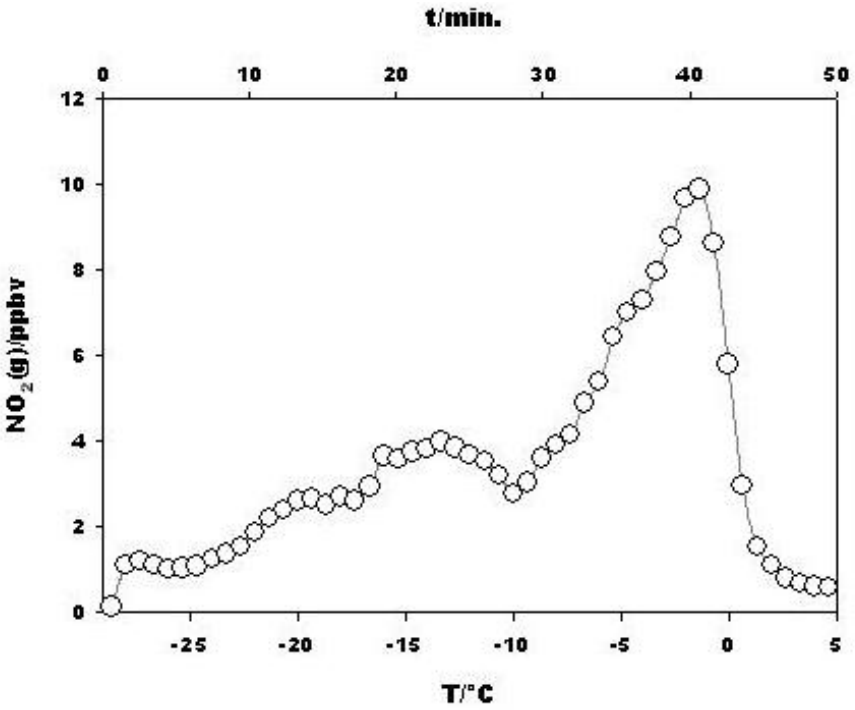

Figure 5.3a. NO_2 gas-phase concentration at ∂H = 0.70 ^{o}C min^{-1} vs. temperature during irradiation of 50 mM nitrate-doped polycrystalline ice.

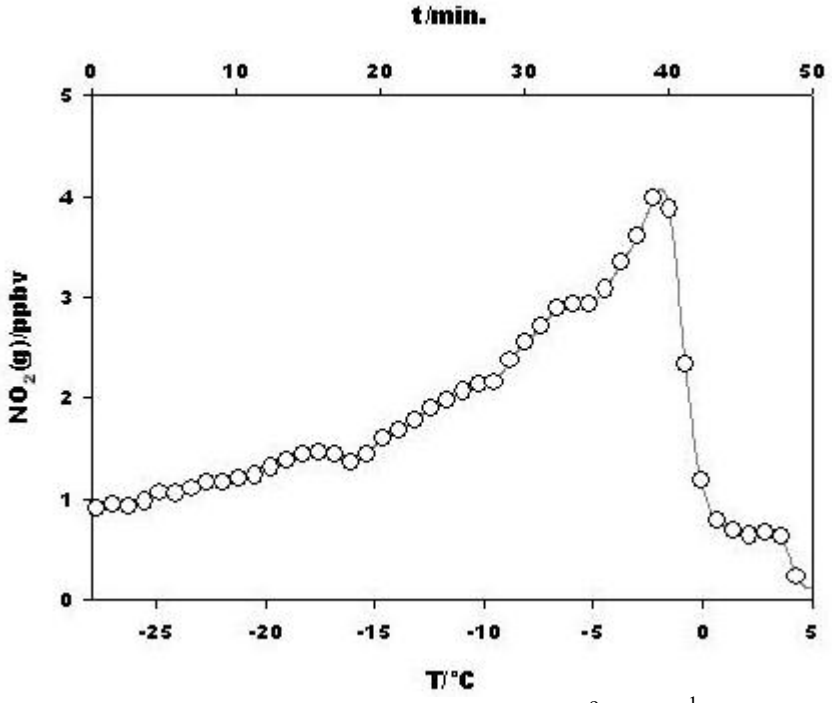

Figure 5.3a. NO_2 gas-phase concentration at ∂H = 0.70 ^{o}C min^{-1} vs. temperature during irradiation of 10 mM nitrate-doped polycrystalline ice.

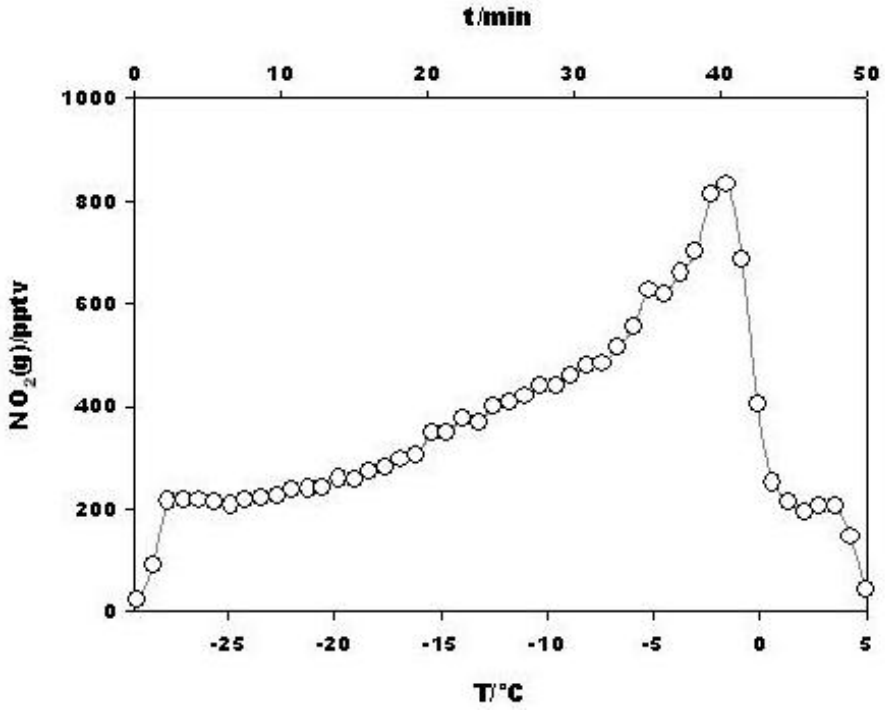

Figure 5.3c. NO_2 gas-phase concentration at ∂H = 0.70 ^{o}C min^{-1} vs. temperature during irradiation of 1 mM nitrate-doped polycrystalline ice.

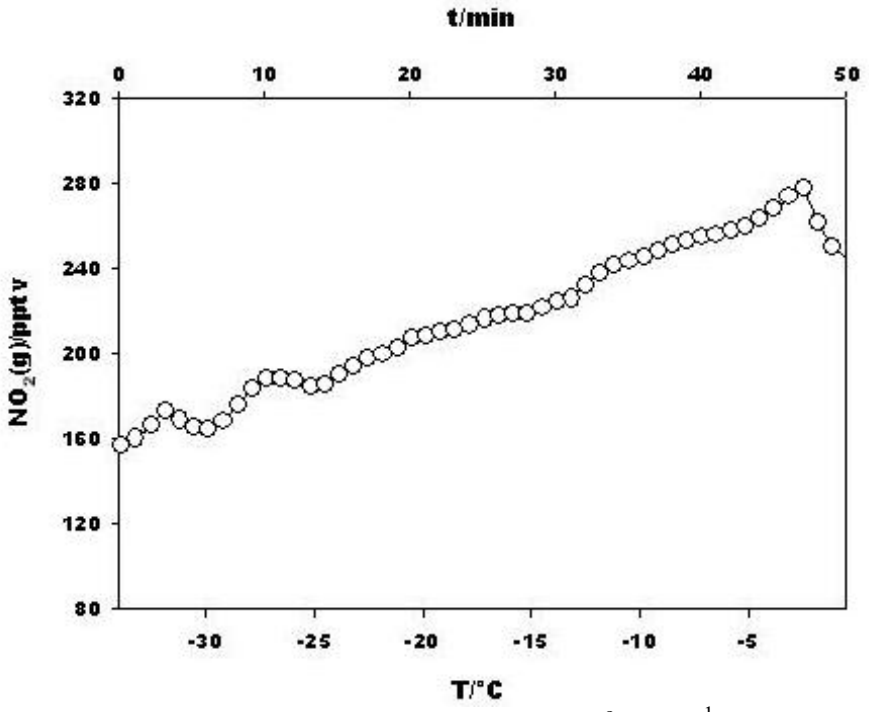

Figure 5.3d. NO_2 gas-phase concentration at ∂H = 0.70 ^{o}C min^{-1} vs. temperature during irradiation of 200 μM nitrate-doped polycrystalline ice.

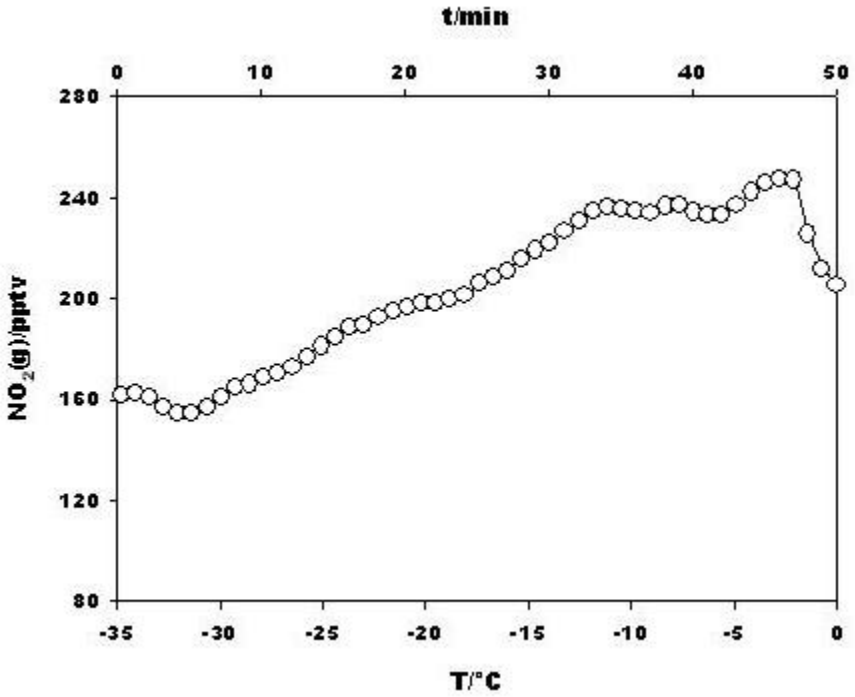

Figure 5.3e. NO_2 gas-phase concentration at ∂H = 0.70 ^{o}C min^{-1} vs. temperature during irradiation of 30 μM nitrate-doped polycrystalline ice.

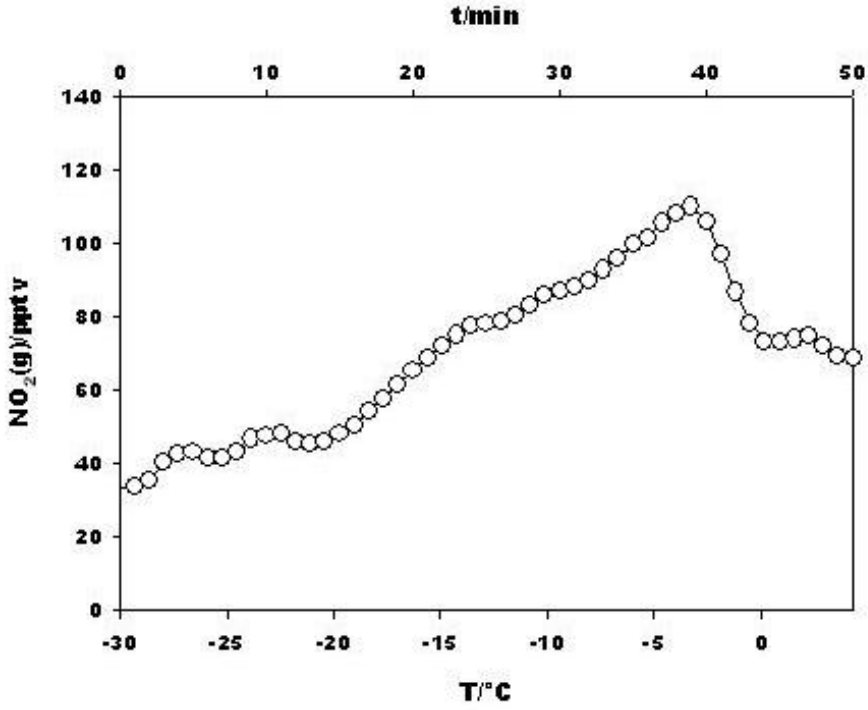

Figure 5.3f. NO_2 gas-phase concentration at ∂H = 0.70 ^{o}C min^{-1} vs. temperature during irradiation of 2 μM nitrate-doped polycrystalline ice.

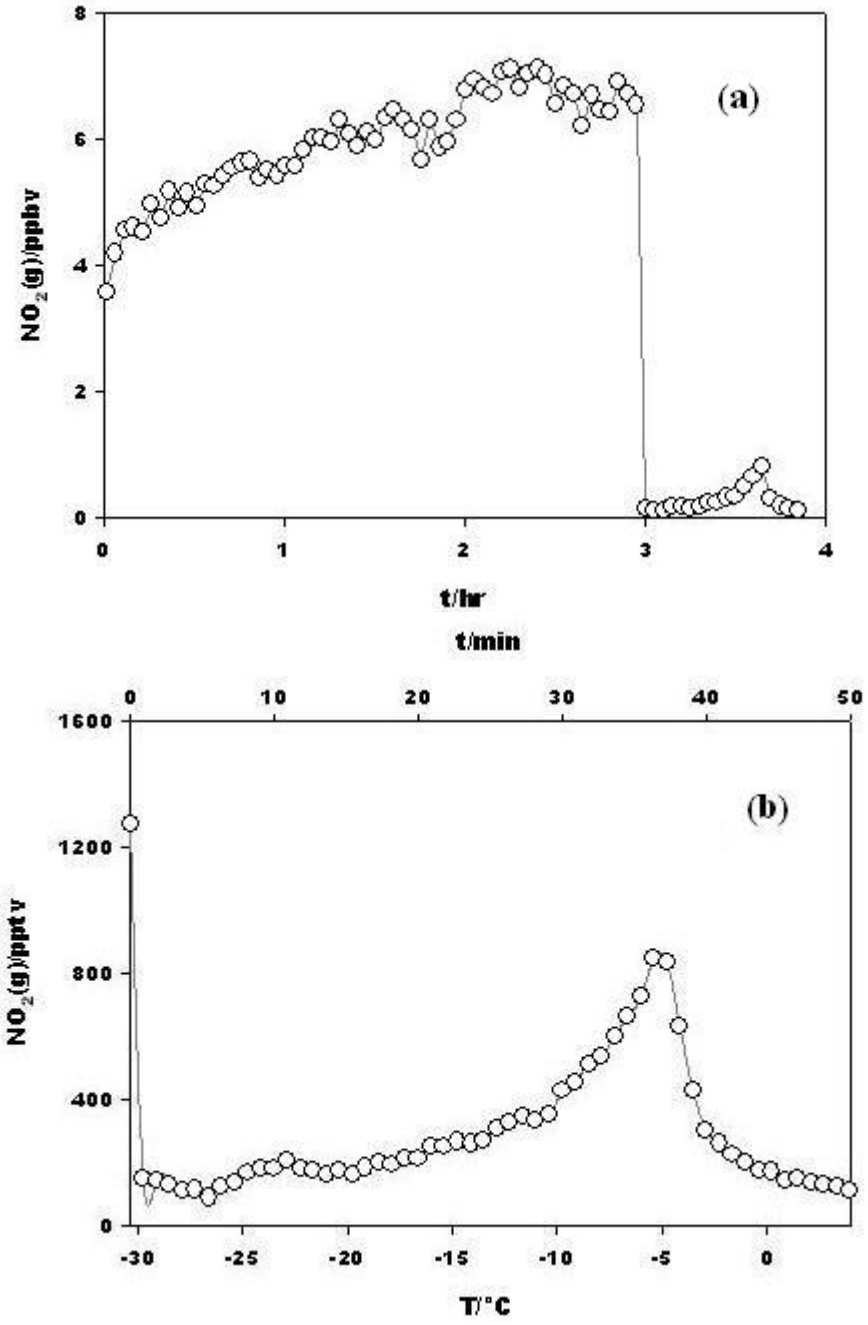

Figures 5.4. (a) NO_2 released from irradiated 50 mM nitrate-doped polycrystalline ice at –30 ^{o}C for 3 - 4 hrs. Subsequently, we observe (b) NO_2 desorption (without photolysis) ∂H = 0.70 ^{o}C min^{-1} ramp rate. Note: fig. (b) rescales both the x- and y-axis of NO_2 desorption data to temperature (T/^{o}C) and pptv., respectively.

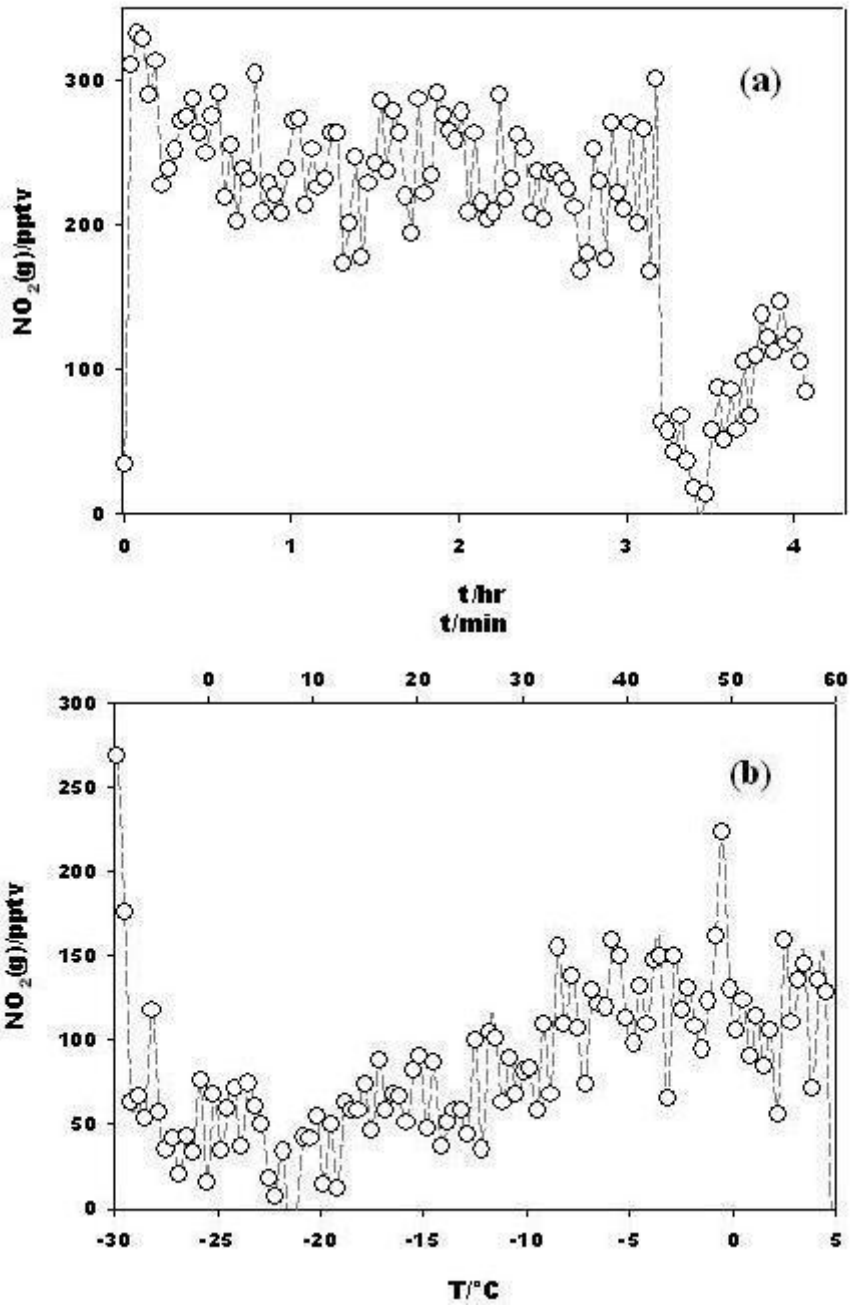

Figure 5.5. (a) NO_2 released from irradiated 2 μM nitrate-doped polycrystalline ice at –30 ^{o}C for 3 – 4 hrs. Subsequently, we observe (b) NO_2 desorption (without photolysis) at $\partial H =$ 0.70 ^{o}C min^{-1} ramp rate. Note: fig. (b) rescales the x-axis of NO_2 desorption data to temperature (^{o}C) .

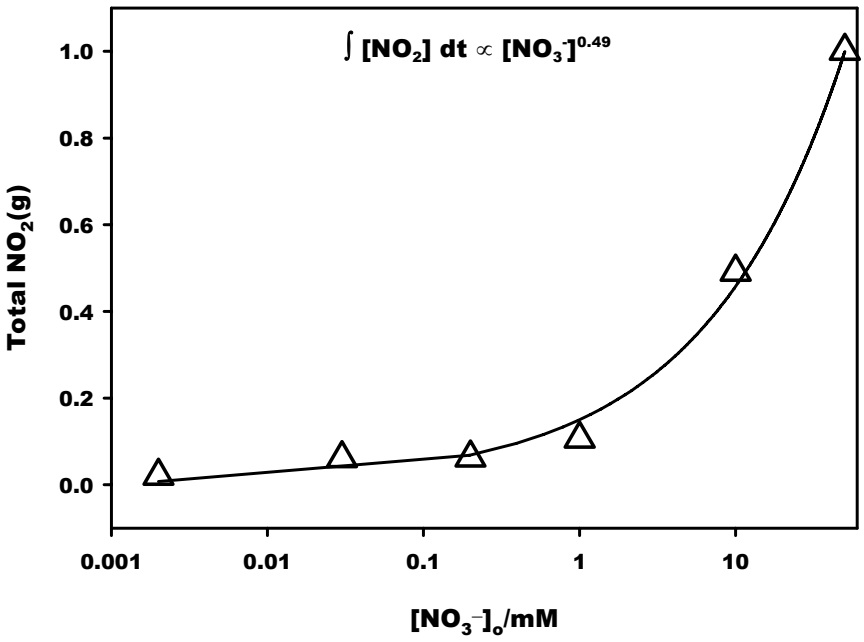

Figure 5.6. Total NO_2 photodesorbed (a.u.) vs. $[NO_3^-]_0$/mM at ∂H = 0.70 ^oC min^{-1} heating rate.

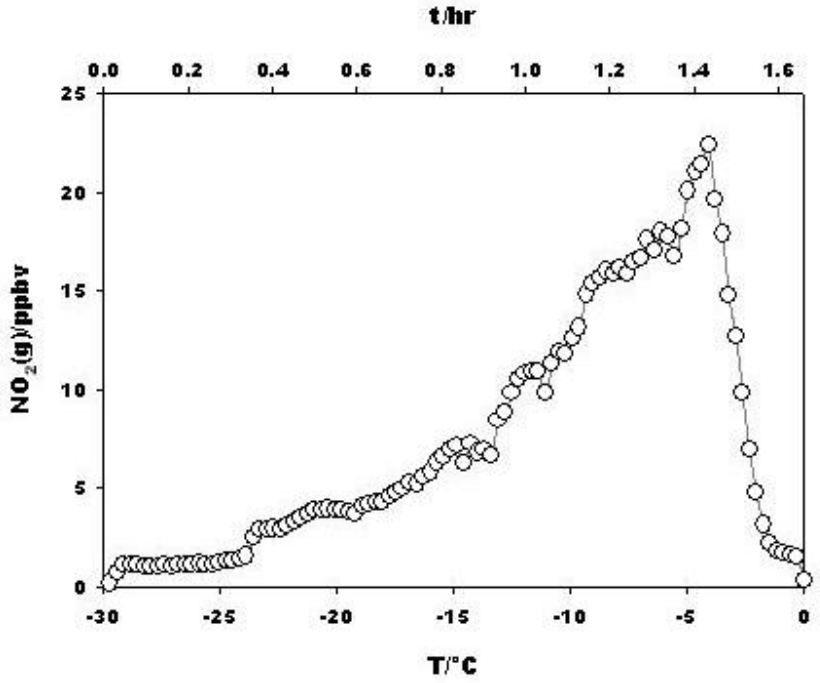

Figure 5.7a. NO_2 released during ∂H = 0.30 ^{o}C min^{-1} ramp rate from irradiated 50 mM nitrate-doped polycrystalline ice vs. temperature.

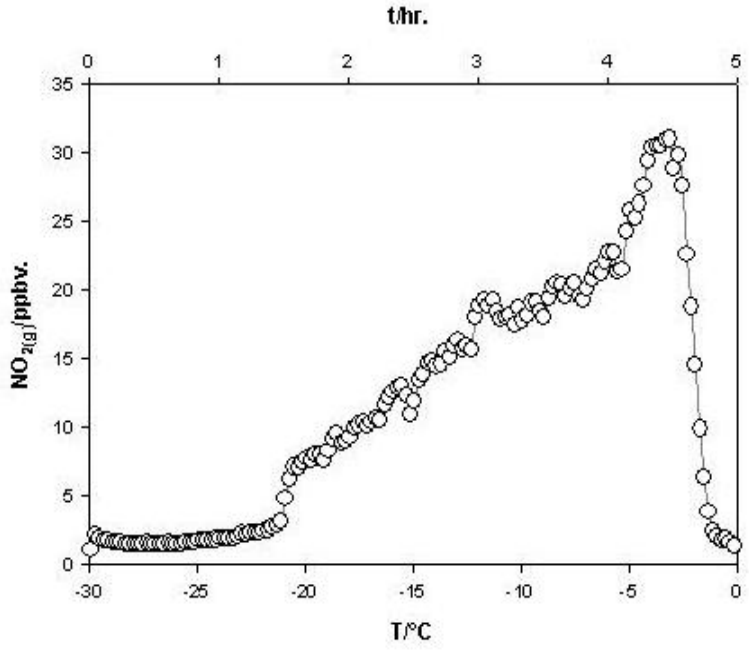

Figure 5.7b. NO_2 released during ∂H = 0.10 ^{o}C min^{-1} ramp rate from irradiated 50 mM nitrate-doped polycrystalline ice vs. temperature.

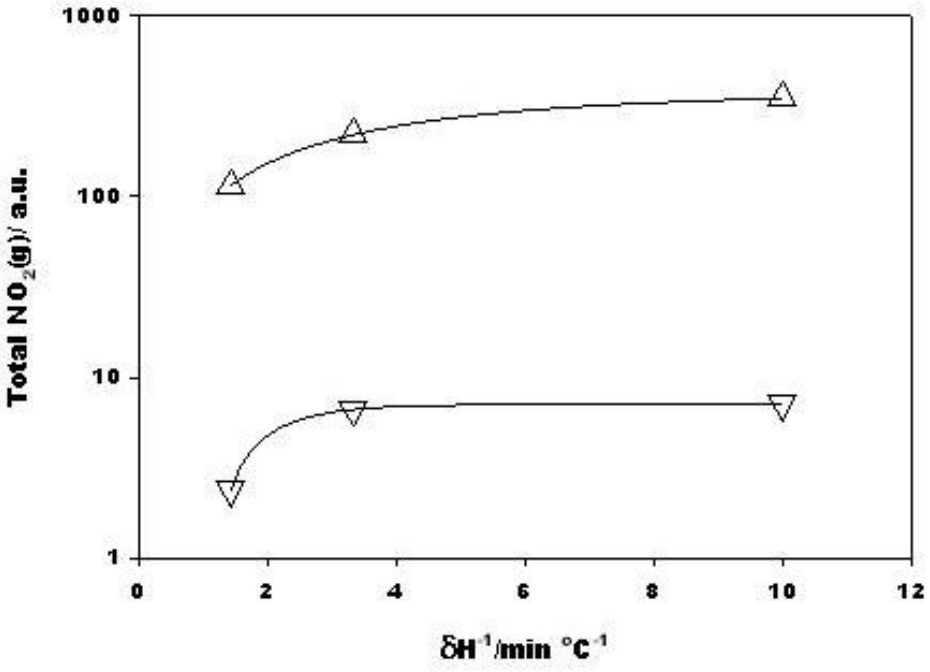

Figure 5.8. Area below curves vs. heating rate (^{o}C min^{-1}) for $[NO_3^-]_0$ = 2 μM (∇) and 50 mM (Δ).

References

(1) Platt, U. *The Origin of Nitrous and Nitric Acid in the Atmosphere*; Springer-Verlag: New York, **1986**; Vol. G6.

(2) Logan, J. A. *J. Geophys. Res.* **1983**, *88*, 10785.

(3) Mulvaney, R.; Wagenbach, D.; Wolff, E. W. *J. Geophys. Res.* **1998**, *103*, 11021.

(4) Legrand, M.; Mayewski, P. *Rev. Geophys.* **1997**, *35*, 219.

(5) Dibb, J. E.; Talbot, R. W.; Munger, J. W.; Jacob, D. J.; Fan, S. M. *J. Geophys. Res.* **1998**, *103*, 3475.

(6) Wolff, E. W. *Nitrate in Polar Ice*; Springer-Verlag: New York, **1995**; Vol. I30.

(7) Beine, H. J.; Domine, F.; Ianniello, A.; Nardino, M.; Allegrini, I.; Teinila, K.; Hillamo, R. *Atmos. Chem. Phys.* **2003**, *3*, 335.

(8) Beine, H. J.; Domine, F.; Simpson, W.; Honrath, R. E.; Sparapani, R.; Zhou, X. L.; King, M. *Atmos. Environ.* **2002**, *36*, 2707.

(9) Beine, H. J.; Honrath, R. E.; Domine, F.; Simpson, W. R.; Fuentes, J. D. *J. Geophys. Res.* **2002**, *107*.

(10) Dibb, J. E.; Arsenault, M.; Peterson, M. C.; Honrath, R. E. *Atmos. Environ.* **2002**, *36*, 2501.

(11) Honrath, R. E.; Lu, Y.; Peterson, M. C.; Dibb, J. E.; Arsenault, M. A.; Cullen, N. J.; Steffen, K. *Atmos. Environ.* **2002**, *36*, 2629.

(12) Davis, D.; Nowak, J. B.; Chen, G.; Buhr, M.; Arimoto, R.; Hogan, A.; Eisele, F.; Mauldin, L.; Tanner, D.; Shetter, R.; Lefer, B.; McMurry, P. *Geophys. Res. Lett.* **2001**, *28*, 3625.

(13) Peterson, M. C.; Honrath, R. E. *Geophys. Res. Lett.* **2001**, *28*, 511.

(14) Ridley, B.; Walega, J.; Montzka, D.; Grahek, F.; Atlas, E.; Flocke, F.; Stroud, V.; Deary, J.; Gallant, A.; Boudries, H.; Bottenheim, J.; Anlauf, K.; Worthy, D.; Sumner, A. L.; Splawn, B.; Shepson, P. *J. Atmos. Chem.* **2000**, *36*, 1.

(15) Jones, A. E.; Weller, R.; Wolff, E. W.; Jacobi, H. W. *Geophys. Res. Lett.* **2000**, *27*, 345.

(16) Honrath, R. E.; Peterson, M. C.; Guo, S.; Dibb, J. E.; Shepson, P. B.; Campbell, B. *Geophys. Res. Lett.* **1999**, *26*, 695.

(17) Chu, L.; Anastasio, C. *J. Phys. Chem. A.* **2003**, *107*, 9594.

(18) Mack, J.; Bolton, J. R. *J. Photochem. Photobiol. A-Chem.* **1999**, *128*, 1.

(19) Mark, G.; Korth, H. G.; Schuchmann, H. P.; vonSonntag, C. *J. Photochem. Photobiol. A-Chem.* **1996**, *101*, 89.

(20) Alif, A.; Boule, P. *J. Photochem. Photobiol. A-Chem.* **1991**, *59*, 357.

(21) Zellner, R.; Exner, M.; Herrmann, H. *J. Atmos. Chem.* **1990**, *10*, 411.

(22) Warneck, P.; Wurzinger, C. *J. Phys. Chem.* **1988**, *92*, 6278.

(23) Zepp, R. G.; Hoigne, J.; Bader, H. *Environ. Sci. Technol.* **1987**, *21*, 443.

(24) Domine, F.; Shepson, P. B. *Science* **2002**, *297*, 1506.

(25) Honrath, R. E.; Peterson, M. C.; Dziobak, M. P.; Dibb, J. E.; Arsenault, M. A.; Green, S. A. *Geophys. Res. Lett.* **2000**, *27*, 2237.

(26) Sumner, A. L.; Shepson, P. B. *Nature* **1999**, *398*, 230.

(27) Bilski, P.; Chignell, C. F.; Szychlinski, J.; Borkowski, A.; Oleksy, E.; Reszka, K. *J. Am. Chem. Soc.* **1992**, *114*, 549.

(28) Boxe, C. S.; Colussi, A. J.; Hoffmann, M. R.; Tan, D.; Mastromarino, J.; Case, A. T.; Sandholm, S. T.; Davis, D. D. *J. Phys. Chem. A.* **2003**, *107*, 11409.

(29) Dubowski, Y.; Colussi, A. J.; Boxe, C.; Hoffmann, M. R. *J. Phys. Chem. A.* **2002**,

106, 6967.

(30) Dubowski, Y.; Colussi, A. J.; Hoffmann, M. R. *J. Phys. Chem. A*. **2001**, *105*, 4928.

(31) Thornton, J. A.; Wooldridge, P. J.; Cohen, R. C. *Anal. Chem.* **2000**, *72*, 528.

(32) Calvert, J.; Pitts, J. N. *Photochemistry*; Wiley: New York, **1966**.

(33) Rempel, A. W.; Waddington, E. D.; Wettlaufer, J. S.; Worster, M. G. *Nature* **2001**, *411*, 568.

(34) Killawee, J. A.; Fairchild, I. J.; Tison, J. L.; Janssens, L.; Lorrain, R. *Geochim. Cosmochim. Acta* **1998**, *62*, 3637.

(35) Takenaka, N.; Ueda, A.; Daimon, T.; Bandow, H.; Dohmaru, T.; Maeda, Y. *J. Phys. Chem.* **1996**, *100*, 13874.

(36) Dash, J. G.; Fu, H. Y.; Wettlaufer, J. S. *Rep. Prog. Phys.* **1995**, *58*, 115.

(37) Gross, G. W.; Gutjahr, A.; Caylor, K. *J. Physique* **1987**, *48*, 527.

(38) Gross, G. W.; Wong, P. M.; Humes, K. *J. Chem. Phys.* **1977**, *67*, 5264.

(39) Gross, G. W.; McKee, C.; Wu, C. H. *J. Chem. Phys.* **1975**, *62*, 3080.

(40) Gross, G. W. *Adv. Chem. Series* **1968**, 27.

(41) Ewing, G. E. *J. Phys. Chem. B* **2004**, *108*, 15953.

(42) Menzel, M. I.; Han, S. I.; Stapf, S.; Blumich, B. *J. Magn. Res.* **2000**, *143*, 376.

(43) Cho, H.; Shepson, P. B.; Barrie, L. A.; Cowin, J. P.; Zaveri, R. *J. Phys. Chem. B* **2002**, *106*, 11226.

(44) Henson, B. F.; Robinson, J. M. *Phys. Rev. Lett.* **2004**, *92*, 246107.

(45) Hindmarsh, J. P.; Buckley, C.; Russell, A. B.; Chen, X. D.; Gladden, L. F.; Wilson, D. I.; Johns, M. L. *Chem. Eng. Sci.* **2004**, *59*, 2113.

(46) Fukazawa, H.; Sugiyama, K.; Mae, S. J.; Narita, H.; Hondoh, T. *Geophys. Res.*

Lett. **1998**, *25*, 2845.

(47) Nye, J. F. *J. Glaciol.* **1989**, *35*, 17.

(48) Mulvaney, R.; Wolff, E. W.; Oates, K. *Nature* **1988**, *331*, 247.

(49) Schwartz, S. E.; White, W. H. *Adv. Environ. Sci. Eng.* **1981**, *4*, 1.

(50) Miura, Y.; Hamada, H. *J. Chromatogr. A* **1999**, *850*, 153.

(51) Li, S. *Atmos. Environ.* **1993**, *27A*, 2959.

(52) Schwartz, S. E.; White, W. H. *Adv. Environ. Sci. Technol.* **1983**, *12*, 1.

(53) De Angelis, D.; Legrand, M. *Ice Core Studies of Global Biogeochemical Cycles, NATO ASI Ser., Ser. 1* **1995**, *30*, 361.

(54) Silvente, E.; Legrand, M. *Ice Core Studies of Global Biogeochemical Cycles, NATO ASI Ser., Ser. 1* **1995**, *30*, 225.

(55) Jaffe, D. A.; Zukowski, M. D. *Atmos. Environ.* **1993**, *27*, 2935.

(56) Stottlemyer, R.; Toczydlowski, D. *Can. J. Fish. Aquat. Sci.* **1990**, *47*, 290.